University of Massachusetts Medical School

eScholarship@UMMS

Senior Scholars Program

School of Medicine

2005-06-01

Magnetic Resonance Imaging of Anatomical Layer Specificity in the Cat Retina

Thomas F. Chang
University of Massachusetts Medical School

Let us know how access to this document benefits you.

Repository Citation

Original Research

Magnetic Resonance Imaging of Tissue and Vascular Layers in the Cat Retina

Qiang Shen, PhD,[1] Haiying Cheng, PhD,[1] Machelle T. Pardue, PhD,[2] Thomas F. Chang, MD,[3] Govind Nair, MS,[1] Van Toi Vo, PhD,[4] Ross D. Shonat, PhD,[5] and Timothy Q. Duong, PhD[1]*

Purpose: To report the visual resolution of multiple cell and vascular "layers" in the cat retina using MRI.

Materials and Methods: T_2- and diffusion-weighted MRI at 4.7 Tesla was performed. Layer-specific thickness, T_2, spin density, apparent diffusion coefficient perpendicular ($ADC_\perp$) and parallel ($ADC_\parallel$) to the retinal surface were tabulated. T_1-weighted MRI was acquired before and after intravenous administration of Gd-DTPA and subtraction images were obtained. Histology was performed for validation.

Results: Three distinct "layers" were observed. The inner strip nearest to the vitreous (exhibiting large T_2, ADC, spin density with Gd-DTPA enhancement) overlapped the ganglion cell layer, bipolar cell layer, and the embedded retinal vascular layer. The middle strip (exhibiting small T_2, ADC, spin density without Gd-DTPA enhancement) overlapped the photoreceptor cell layer and the inner and outer segments. The outer strip (exhibiting large T_2, ADC, spin density with Gd-DTPA enhancement) overlapped the tapetum and choroidal vascular layer. T_2, spin density, $ADC_\perp$ and $ADC_\parallel$ of different "layers" were tabulated. The inner strip was slightly thicker than the other two strips. The total thickness, including neural and nonneural retina, was $358 \pm 13\mu m$ ($N = 6$) by MRI and $319 \pm 77 \ \mu m$ ($N = 5$) by histology.

Conclusion: MRI provides a noninvasive tool to study the retina with laminar specificity without depth limitation.

THE RETINA IS HIGHLY STRUCTURED and is composed of three major cell layers: photoreceptors layer, bipolar cell layer, and ganglion cell layer (see Fig. 1) (1). The plexiform layers are synaptic links between adjacent nuclear cell layers. Histological studies suggest that the cell density is highest in the photoreceptor layer of the retina (2). In cat, there is a tapetum (3), a tissue layer that is located beneath the retinal pigment epithelium and serves to reflect light back to the retina to improve vision in low light conditions.

The retina is nourished by two separate blood supplies: the retinal and choroidal vasculatures (4) on either side of the retina. The retinal vasculature exists primarily within the ganglion cell layer, but does project a deep planar capillary bed into the bipolar cell layer. The choroidal vasculature does not exist within any retinal layer, but rather is located directly beneath the photoreceptor layer, sandwiched between the tapetum and the sclera in cat. Thus, the outer nuclear (photoreceptor) layer is completely avascular (4) and relies on both vasculatures for the delivery of oxygen and nutrients. The tapetum is vascularized by the choroidal vasculature. While the mammalian retina requires both the retinal and choroid vasculatures for proper function, there are marked differences between them. Choroid blood flow is many times higher than retinal blood flow and is generally much less responsive to blood flow modulating factors (2,5). Some diseases of the eye, including diabetic retinopathy (6,7), glaucoma (8) and macular degeneration (9,10), have differential effects on different vascular and/or tissue layers. Thus, the ability to non-invasively resolve retinal tissue layers, including the two distinct vascular layers, could have many important applications.

The retina has been studied using many different techniques. Electroretinography (11,12) is widely used to study retinal electrical activity and function. Oxygenation and oxygenation changes in the retina have been studied using oxygen electrodes (13,14), phosphores-

[1]Yerkes Imaging Center, Division of Neuroscience, Department of Neurology, Emory University, Atlanta, Georgia, USA.

[2]Department of Ophthalmology, Emory University and Rehabilitation Research and Development, Atlanta VA Medical Center, Atlanta, Georgia, USA.

[3]University of Massachusetts School of Medicine, Worcester, Massachusetts, USA.

[4]Department of Biomedical Engineering, Tufts University, Medford, Massachusetts, USA.

[5]Department of Biomedical Engineering, Worcester Polytechnic Institute, Worcester, Massachusetts, USA.

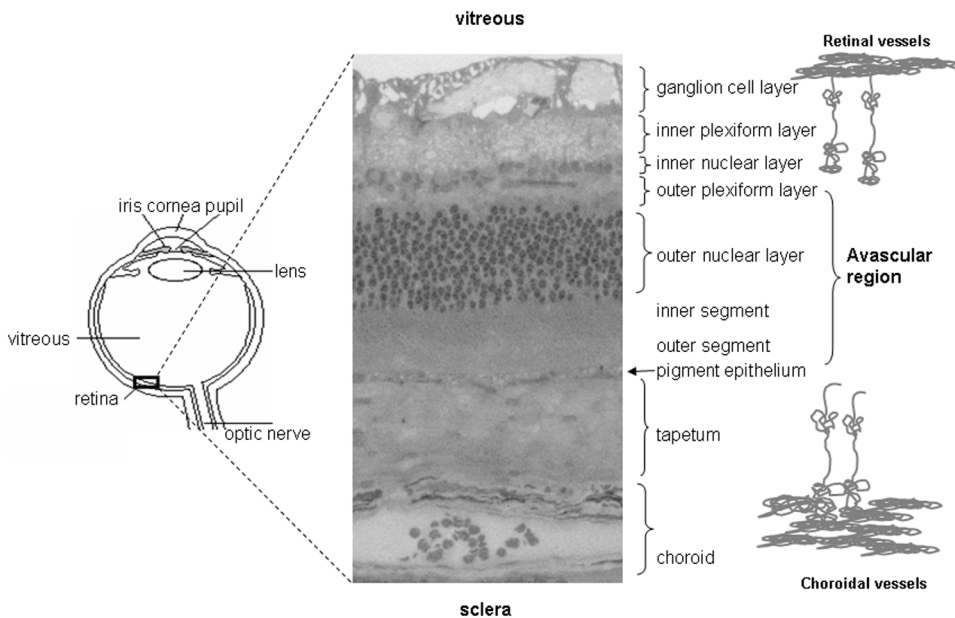Qiang Shen and Haiying Cheng contributed equally to this work.

Figure 1. Histological section of the retina. Different cell layers, tapetum, retinal and choroidal vessels are depicted. The retinal vasculature exists primarily within the inner ganglion cell layer, but does project a deep planar capillary bed into the bipolar cell layer. The choroid vasculature does not exist within any retinal layer, but rather is located directly beneath the photoreceptor layer, sandwiched between the tapetal cell layer and the sclera. The photoreceptor layer is avascular.

cence (15), and, more recently, intrinsic optical imaging technique (16–18). Several methods also exist for measuring blood flow in the retina, including fluorescein angiography (19,20) which can measure retinal circulation and indocyanine-green angiography (21,22) which can measure choroidal circulation in the fovea. Confocal imaging (23) and optical coherence tomography (24,25) are widely used to measure retinal thickness. While most of these optical techniques offer high temporal and spatial resolution, strong tissue absorption of visible light could be problematic in the deeper layers, particularly the retinal pigment epithelial, tapetum, and choroid vascular layer. Furthermore, disease-induced opacity of the vitreous humor, cornea and/or lens (such as cataract) could render the use of these and other optical techniques less effective.

MRI is a powerful tool for diagnostic imaging because it provides noninvasive, three-dimensional high-resolution anatomical images with excellent soft-tissue contrast without depth limitation. Typical anatomical MRI contrasts arise from differences in water spin density, relaxation times, and/or apparent diffusion coefficient (ADC). Water relaxation times (such as T_1 and T_2) are dependent on the local biophysical and biochemical environments. Water displacement in biological tissues is restrictive and anisotropic due to the presence of semipermeable cell membranes, macromolecules and organelles. Thus, different tissue types have different water spin density, T_1, T_2, and ADC, giving rise to MRI contrasts. In addition, MRI contrasts can be enhanced using an exogenous MRI contrast agent. Gadolinium-diethylene-tri-amine-pentaacetic acid (Gd-DTPA or Magnevist®) is a biologically stable, nontoxic, compartment-specific MRI contrast agent which shortens water T_1, and it has been widely used in animals and humans. Blood vessels in the brain and the retina are impermeable to Gd-DTPA due to the presence of the blood–brain and blood–retina barriers, respectively. Thus, enhancement is localized to the intravascular space. One unique advantage of MRI is that anatomy, physiology (such as tissue blood flow and oxygenation), metabolism, and function can be studied in the same setting non-invasively and in a longitudinal fashion.

Oxygenation changes (ΔPO_2 technique) in the vitreous humor near the retina had been reported by measuring T_1 changes of ^{19}F perfluorocarbon droplets injected into the vitreous (26) and endogenous water in the vitreous (27) based on the paramagnetic property of dissolved O_2. More recently, blood-oxygenation-level-dependent (BOLD) functional fMRI (28), which is widely used to study brain functions and physiology, has also been extended to study the retina in association with visual stimuli and physiological challenges (29,30). However, MRI studies of the retina to date have relatively low spatial resolution and/or contrast-to-noise ratio and lamina-specific MRI of the retina has not been reported.

The goal of this study was to explore T_2, diffusion, and Gd-DTPA contrast-enhanced T_1 imaging to resolve tissue and vascular layers in the retina. Laminar-specific thickness, T_2, spin density, ADC parallel and perpendicular ($ADC_\parallel$ and $ADC_\perp$) to the retinal surface of different retinal "layers" were tabulated. Histology was performed for validation.

MATERIALS AND METHODS

Experimental Designs

Multiple MRI survival experiments were performed on five female adolescent cats (0.7–1.4 kg) with institutional approval and in accordance with the guidelines for the Use of Animals in Ophthalmic and Vision Research. The cat model and setup for MRI studies has been detailed elsewhere (29,31). Briefly, cats were anesthetized intramuscularly with a ketamine (10–25 mg/kg) and xylazine (2.5 mg/kg) mixture. The animal was intubated and mechanically ventilated using a Harvard ventilator under isoflurane anesthesia (1.25–1.50%) in humidified air throughout the experiment. With this
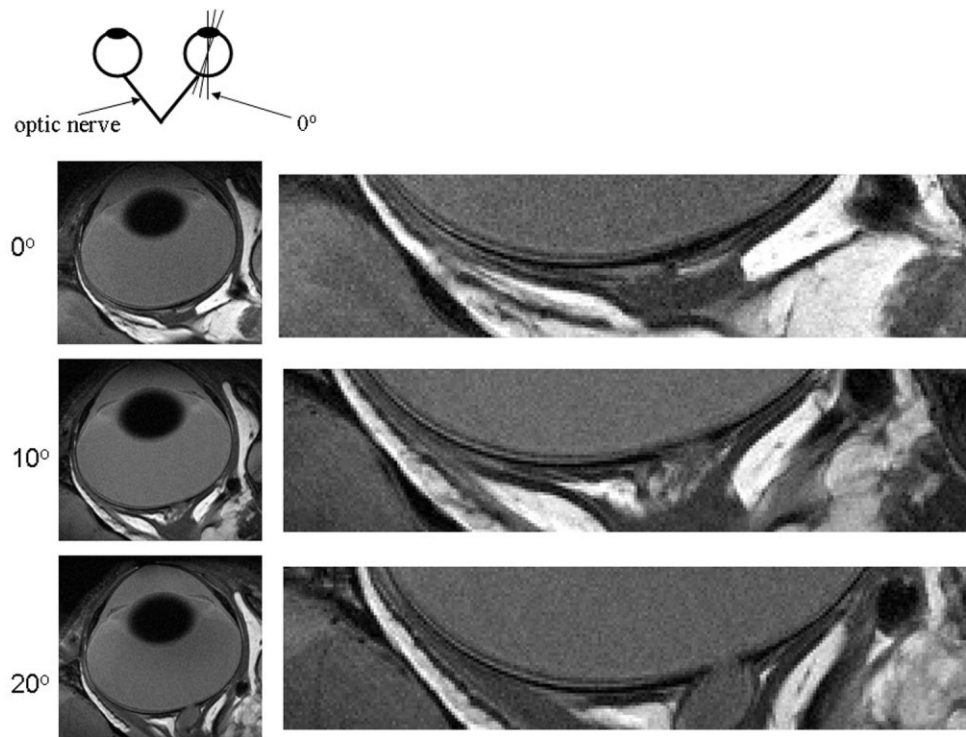
Figure 2. T_2-weighted (TE = 40 msec) images at 100×100 μm^2 resolution at three different radial slice orientations. Image at $0°$ is the sagittal slice (center of the eye) and images at $10°$ and $20°$ extend toward the optic nerve (right eye). The right panels show expanded views.

anesthetic level, we did not observe significant saccade drift. End-tidal CO_2 was continuously monitored using a capnometer (Surgivet, Waukesha, WI, USA) and kept within normal physiological ranges (~4%, via an ~8-ft line). Subcutaneous fluid supplement, topical anesthetic and ophthalmic gel were administered. The animal was then placed in a cradle and restrained in a normal postural position using a head holder consisting of ear, eye, and mouth bars. The animal's rectal temperature was maintained at $38.0 \pm 0.5°C$ throughout the experiments. For contrast-enhanced imaging, Gd-DTPA (Berlex Lab, Montville, NJ, USA) was administered intravenously (0.4 mL/kg from a standard 0.5 M bottle) via the catheterized vein of the forearm.

Six T_2 and diffusion studies were performed at low (100×100 μm) resolution and four at high (50×100 μm) resolution. Six contrast-enhanced T_1 imaging studies were performed. On a given day, multiples of these protocols (T_2 and diffusion imaging at high or low resolution, and/or T_1 imaging) were performed on each animal lasting 6–8 hours, including animal preparation.

MRI Experiments

MRI experiments were carried out on a 4.7-Tesla, 40-cm horizontal MRI scanner, equipped with a 20-Gauss/cm gradient (12 cm inner diameter, 120 μsec rise time; Bruker, Billerica, MA, USA), and a Bruker console (Billerica, MA, USA). A custom-built, small elliptical surface coil (2.5×2.0 cm^2) was placed lateral to the right eye.

T_2-weighted images were acquired using the fast spin-echo (RARE) pulse sequence. First, scout T_2-weighted images with a single TE of 40 msec were acquired at different angles rotating $\pm 30°$ about the mid-

sagittal slice in steps of $10°$ (Fig. 2). Subsequent T_2-weighted images were acquired using multiple TE. The MR parameters were: repetition time (TR) = 4000 msec ($90°$ flip angle), effective echo time (TE) = 40, 52, 72, and 100 msec, spectral width = 50 kHz, 32 segments (eight echoes per segment), three 1.5-mm midsagittal slices roughly bisecting the area centralis, eight averages, field of view (FOV) = 2.56 cm $\times$ 2.56 cm, data matrix = 256×256, and 100×100 μm^2 in-plane resolution.

Diffusion-weighted images (DWI) were acquired with diffusion-sensitive gradients applied along the x, y, or z direction separately. The imaging parameters were TR = 2500 msec ($90°$ flip angle), TE = 43 msec, three 1.5-mm slices, duration between applications of two diffusion gradient pulses (Δ) = 20 msec, diffusion gradient pulse duration (δ) = 3.5 msec, b-value = 6, 504 seconds/mm^2, two averages, FOV = 2.56×2.56 cm^2, matrix size = 256×256, and 100×100 μm^2 in-plane resolution. The 504 seconds/mm^2 b-value, which is smaller than that typically used in brain imaging, was chosen to approximate the e-fold signal attenuation for the retina and optimal visual contrast.

T_1-weighted images were acquired using RARE acquisition with the same parameters as the T_2 imaging above except a shorter TR = 1500 msec ($90°$ flip angle), and eight averages, effective TE = 40 msec (albeit some T_2-weighting which was useful for comparison; its T_2 contribution could be removed by pre- and post-contrast subtraction).

In some T_2, diffusion and T_1 imaging studies, 50×100 μm^2 in-plane resolution was also acquired in which the readout FOV was reduced by half.

Data Analysis

T_2 maps were calculated pixel-by-pixel using, $S(TE) = S_o \cdot exp(-TE/T2)$, where TE is the effective echo time at the center of the echo-train length, and S_o is the signal intensity at TE = 0. T_2 and S_o were derived using non-linear least squared regression with Matlab codes.

ADC maps with intensity in unit of mm^2/second were calculated pixel-by-pixel by using two b-values (6 and 504 seconds/mm^2) and the equation, $S(b_i) = S_o \cdot exp[-b_i \cdot ADC]$, where $b_i = \gamma^2 G_i^2 \delta^2 (\Delta - \delta/3)$, S_o is the signal intensity obtained with b = 0. The b-value is proportional to the gradient strength (G), magnetogyric ratio (γ), duration of each gradient pulse (δ), and the time (Δ) between applications of the two gradient pulses. The S_o maps at b = 0 were also calculated. ADC maps were calculated with correction for cross-term interaction between diffusion and imaging gradients.

DWI along three principal axes (DWI_x, DWI_y, and DWI_z), T_2-weighted images, ADC maps along different axes, T_2 maps, and effective spin-density maps extrapolated from the ADC and T_2 measurements were analyzed for their ability to delineate retinal tissue layers. DWI_z corresponded to the diffusion gradient perpendicular to the retinal surface ($DWI_\perp$) at the back of the eye; DWI_x and DWI_y corresponded to the diffusion gradient parallel to the retinal surface at the back of the eye ($DWI_\parallel$). Note that TR used herein did not allow full T_1 recovery (particularly for the vitreous) and thus the S_o derived in this study was referred to as "effective" spin-density S_o maps.

Pixel-by-pixel subtraction was made between T_1-weighted images acquired before and after Gd-DTPA injection.

Group-averaged T_2, S_o, $ADC_\perp$, and $ADC_\parallel$ of different "layers" of the retina, the vitreous humor and the muscles around the eye as well as retinal thickness for each "layer" were tabulated.

Histology

Histology was obtained on a separate group of animals (N = 5). Following anesthetic overdose (Pentobarbital, 207 mg/kg), eyes were enucleated and immersion fixed overnight in 2% paraformaldehyde/2.5% glutaraldehyde. Eyes were rinsed in 0.1 M phosphate buffer, dissected to isolate the posterior eyecup, divided into 3 mm × 2 mm pieces, and embedded in epoxy-resin (Embed 812, Electron Microscopy Services, Fort Washington, PA, USA). The embedded retinal pieces were sectioned at 0.5 μm, using a histodiamond knife (Diatome, Electron Microscopy Services, Fort Washington, PA, USA) on an ultramicrotome, and stained with toluidine blue. Each histological section was digitally photographed using a Leica Digital camera. Thickness of different layers of the neural retina, tapetum, and choroid vasculature were automatically derived using an image analysis program (Image Pro, Cybernetics). A shrinkage correction factor of 25% was applied as done by Buttery et al (32).

All data are presented in mean ± SD. A P value <0.05 was considered to be statistically significant.

RESULTS

Histology

A representative histological section is shown in Fig. 1. Different cell layers, retinal and choroidal vessels are depicted. The average thickness of the neural retina as determined by histology was 184 ± 32 μm. The tapetum thickness was 86 ± 35 μm, and choroid vascular thickness was 82 ± 14 μm (N = 5, mean ± SD). The total thickness, including the neural retina, tapetum, and choroid was 319 ± 77 μm.

T_2 Imaging

Figure 2 shows the T_2-weighted images at 100 × 100 μm^2 resolution for three different radial slice orientations with respect to the center of the eye. Multiple "layers" were observed in the retina, as indicated by the alternating bright, dark and bright strips on the T_2-weighted images. These laminar structures disappeared in and around the optic nerve head. The retinal surface surrounding the optic nerve head protruded slightly and showed slightly different contrast, consistent with its known structure. There was no indentation around the area centralis on the T_2-weighted images because the cat does not have a fovea (2), in contrast to the human's fovea where the retina becomes thinner relative to surrounding regions.

The T_2-weighted image, T_2 map, and S_o map of the retina at 100 × 100 μm^2 in-plane resolution are displayed in Fig. 3 (midsagittal view). Multiple tissue "layers" in the retina were consistently observed in every animal. The zoomed-in region of the retina showed approximately four 100-μm pixels or approximately three diagonal 100-μm pixels spanning across the retinal thickness. The "inner" strip closest to the vitreous appeared slightly thicker than the other two strips. Similarly, T_2 map showed the bright, dark and bright strips corresponding to tissue layers with long, short and long T_2, respectively. The effective S_o maps showed the corresponding high, low and high water spin density.

Diffusion Imaging

To further investigate the resolution of the retinal layers, diffusion imaging with diffusion-sensitizing gradients along three principal directions was performed (Fig. 4; 100 × 100 μm^2). With diffusion gradient perpendicular to the retina surface at the back of the eye ($DWI_\perp$, z-axis), alternating bright, dark and bright strips were observed. ADC maps showed the corresponding strips with high, low, and high ADC values, respectively. The effective S_o maps also showed the corresponding high, low and high spin density. Note that bright DWI should yield low ADC but high ADC was observed. This is because the DWI signals were dominated by water spin density.

When the diffusion-sensitive gradient was switched to parallel to the retina surface at the back of the eye ($DWI_\parallel$, x or y axis), different contrast was observed. Specifically, the signal in the outer strip was lower in $DWI_\parallel$ relative to $DWI_\perp$, indicative of anisotropic diffusion. Three strips on the $DWI_\perp$ essentially overlapped the three strips on the T_2-weighted images pixel-by-
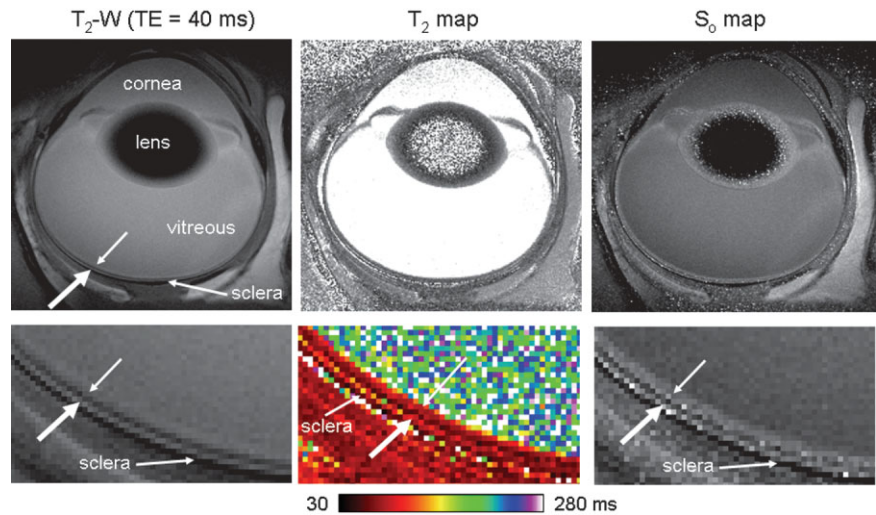
Figure 3. T_2-weighted (TE = 40 msec) images, effective spin-density (S_o) and T_2 maps at 100×100 µm resolution. Image slice was obtained at the middle of the eye, roughly bisecting the area centralis. The small and large white arrows indicate the "inner" and "outer" strips, respectively.

pixel. Diffusion imaging also showed approximately four 100-µm pixels or approximately three diagonal 100-µm pixels spanning across the retinal thickness.

Higher Resolution T_2 and Diffusion Imaging

In some studies, higher spatial resolution (50×100 µm^2) T_2 and diffusion imaging were also performed. Representative images are shown in Fig. 5. Across the thickness of the retina, there were approximately eight 50-µm pixels and three strips were observed, in good agreement with the low-resolution data. In some animals, higher spatial resolution data showed additional anatomical parcellation beyond the three strips. T_2 and ADC of different "layers", however, were not quantified.

Contrast-Enhanced Imaging

To further corroborate the laminar classification, contrast-enhanced imaging was performed with the administration of a blood-pool Gd-DTPA contrast agent (Fig. 6). Precontrast spin-echo T_1-weighted images (with some T_2 weighting) also showed three distinct strips. Spin-echo T_1-weighted images of the retina after Gd-DTPA administration showed marked enhancement of the anterior segment of the eye due to the high Gd-DTPA permeability of the ciliary body. Extraocular enhancement was also observed. Subtraction of post- and precontrast images of two cats showed marked signal enhancement on either side of the retina, with the outer band being more enhanced and appeared thicker than the inner band. In contrast, subtraction images showed no enhancement for the middle of the retina and the vitreous. Enhancement of the "inner" band on the subtraction images essentially overlapped with the "inner" strip of the precontrast images, and the enhancement of the "outer" band on the subtraction images essentially overlapped with the "outer" strip of the precontrast images.

The group-averaged T_2, ADC$_\parallel$ and ADC$_\perp$ of the different strips of the retina and the vitreous humor are summarized in Table 1. T_2 and ADC values of the inner and middle strips of the retina were similar to those of the cortical gray matter. In contrast, the T_2 and ADC values of the outer strip were slightly higher than other strips ($P < 0.05$) and the ADC$_\parallel$ was larger than ADC$_\perp$ in the outer strip ($P < 0.05$). ADC$_\parallel$ across all layers were higher than ADC$_\perp$, indicative of anisotropic diffusion. T_2 and ADC of the vitreous were markedly larger than those of the retinal strips, and the ADC$_\parallel$ and ADC$_\perp$ of the vitreous were not statistically different, as expected. Taken together, the MRI-estimated thickness of the retina was 356 ± 13 µm ($N = 6$) based on low resolution data and ~ 360 µm ($N = 4$) based on high resolution data. The inner strip appear slightly thicker than the middle strip and the outer strip.
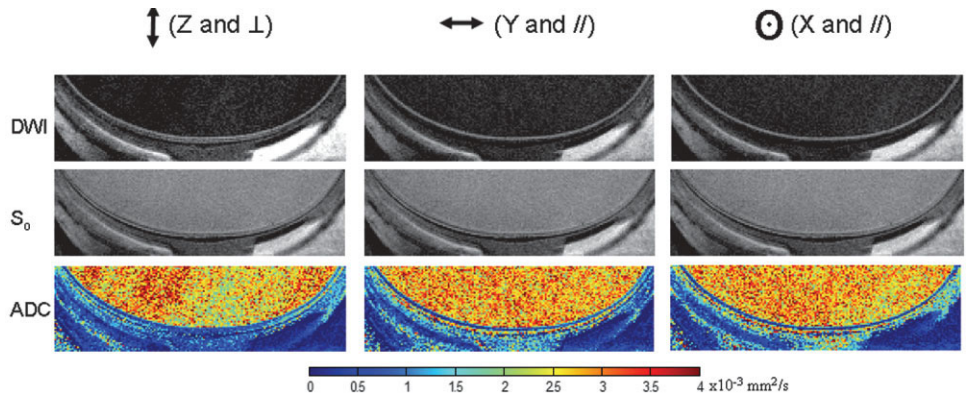

Figure 4. Diffusion-weighted images, ADC and spin-density maps at 100×100 µm^2 resolution. Diffusion-sensitizing gradients were placed along the x, y, or z axis separately. The vertical and horizontal double arrows and concentric circle-and-dot indicate the different directions of the diffusion gradients.
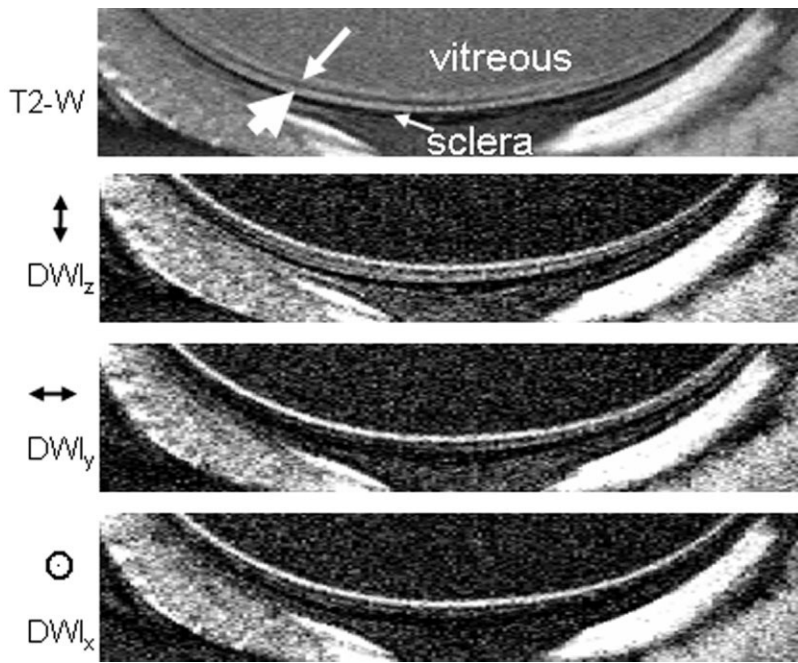
Figure 5. Higher-resolution T_2-weighted (TE = 40 msec) and diffusion-weighted (b = 504 seconds/mm^2) images at 50 × 100 μm resolution. Diffusion-sensitizing gradients were placed along the x, y, or z axis separately. The small and large white arrows indicate the "inner" and "outer" strips, respectively.

DISCUSSION

This study demonstrates the visual resolution of multiple distinct tissue and vascular "layers" in the cat retina using multiple MRI contrast mechanisms. Three major strips were observed. The inner strip nearest to the vitreous, exhibiting long T_2 value, high water spin density, and Gd-DTPA enhancement, likely overlaps the ganglion and bipolar cell layer and the embedded retinal vessels. The middle strip, exhibiting short T_2 value, low water spin density and no significant Gd-DTPA enhancement, likely overlaps the photoreceptor layer, inner and outer segments of the photoreceptors. The outer strip, exhibiting long T_2 values, high water spin density and Gd-DTPA enhancement, likely corresponds to the tapetum and the choroid vascular layer (Fig. 1).

One major disadvantage of MRI for resolving laminar structures in the retina is its limited spatial resolution compared to optical and histological techniques. This led to partial-volume effect which could affect the tabulated data on laminar thickness, T_2, S_o, $ADC_\parallel$, and $ADC_\perp$ of different layers. MRI also has relatively poor temporal resolution compared to many other optical techniques. The unique advantage of MRI, however, is its ability to measure structural, physiological (such as blood flow and oxygenation), metabolic and functional data in a single setting and in a longitudinal fashion, which are generally not feasible with existing tech-
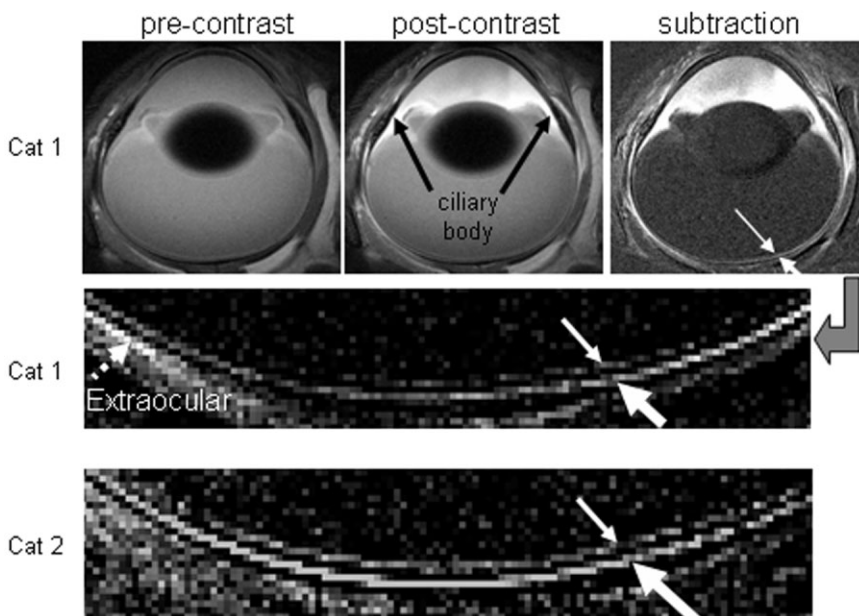

Figure 6. Contrast-enhanced spin-echo T_1-weighted images at 100 × 100 μm. The smaller and larger white arrows indicate the "inner" and "outer" bands, respectively. Two black arrows indicate the ciliary bodies. Extraocular enhancement was also observed (dashed arrow).

Table 1
Group-Average T_2, $ADC_\parallel$ and $ADC_\perp$ Values of the "Inner," "Middle," and "Outer" Strips of the Retina, Vitreous Humor, and Brain Tissues at 4.7 Tesla ($N = 6$, mean $\pm$ SD)

	T_2 (msec)	$ADC_\parallel$ ($\times 10^{-3}$ mm^2/second)	$ADC_\perp$ ($\times 10^{-3}$ mm^2/second)
Vitreous humor	218 ± 12	2.73 ± 0.22	2.66 ± 0.22
Retina			
"Inner"	67 ± 5	1.1 ± 0.2	0.74 ± 0.1
"Middle"	48 ± 5	1.2 ± 0.3	0.67 ± 0.1
"Outer"	95 ± 6	3.3 ± 0.7	1.2 ± 0.2
Muscle around eye[a]	73 ± 8	0.78 ± 0.2	0.75 ± 0.2
Rat brain gray matter	54 ± 2[b]	0.74 ± 0.02[c]	

T_2, $ADC_\parallel$, and $ADC_\perp$ of the vitreous were statistically different ($P < 0.005$) from those of the inner, middle, and outer strips, except between the vitreous and outer strip $ADC_\parallel$.
[a]Muscle at the posterior-dorsal area of the eye was obtained to check for internal consistency.
[b]Unpublished rat data ($N = 7$) obtained using essentially identical sequence parameters as herein.
[c]Average ADC measured along x, y, and z direction separately from rat brain (37).

niques. MRI also has no depth limitation. Therefore, MRI has the potential to complement existing techniques to study the retina.

In the middle strip (part of the neural retina), T_2 and ADC values were smallest among the three strips and were similar to those of the cortical gray matter (see Table 1) but were markedly smaller than those of the vitreous. $ADC_\parallel$ of the middle strip was higher than $ADC_\perp$, indicative of anisotropic diffusion, whereas there was no statistical different between $ADC_\parallel$ and $ADC_\perp$ in the vitreous. This middle strip is most consistent with being the photoreceptor layer because it has the highest macromolecular and cell density and, thus, yield a relative small T_2, ADC, and spin density, relative to the other strips and the vitreous. Furthermore, this middle strip also showed no Gd-DTPA enhancement and is thus avascular, as expected based on known retinal anatomy (4).

In the inner strip (also part of the neural retina), ADC was similar to the middle strip but T_2 was slightly higher relative to the middle strip. The most likely explanation for the T_2 difference is that there is a partial-volume effect with the very large vitreous T_2 (5 times that of the cortical gray matter and the middle strip) and thus a small partial volume effect could readily account for the slightly elevated T_2 of the inner strip, although different tissue MRI properties per se could be a factor. On the contrary, the ADC difference between the inner strip and the vitreous was smaller, leading to less partial-volume effect on the ADC values of the inner strip. $ADC_\parallel$ of the inner strip was also higher than $ADC_\perp$, indicative of anisotropic diffusion. This inner strip is most consistent with being the ganglion cell layer and bipolar cell layer and it is vascularized, as demonstrated by the Gd-DTPA experiments.

In the outer strip, T_2 and ADC values were higher than the middle strip. This strip showed Gd-DTPA enhancement and is vascularized. The outer strip is most consistent with being the choroidal vascular layer and

the tapetum. The large T_2 value in this strip is consistent with the choroid vascular layer and the tapetum being more fluid-like and/or having lower cell and macromolecular density (2). In regard to ADC, $ADC_\parallel$ of the outer strip was also higher than $ADC_\perp$ and both are relatively high compared to those of the middle strip. A likely explanation is that blood flow in the tortuous arteriole and capillary network (33) leads to loss of phase coherence that is indistinguishable from the diffusion process and thus effectively yields a relatively high ADC. The observed anisotropic diffusion characteristics in this strip (e.g., $ADC_\parallel \gg ADC_\perp$) is likely due to water displacement being less restrictive tangential to the outer retinal surface than perpendicular to it (2,5).

Subtraction of post- and precontrast images from the Gd-DTPA experiments showed marked signal enhancement on either side of the retina, with the outer band being more enhanced and appeared thicker than the inner band. This was in contrast to the inner strip which was slightly thicker than the outer strip on pre-Gd-DTPA T_2-weighted images. The contrast-enhanced imaging results indicated that: 1) There are two vascular layers located at either end of the retina with the middle of the retina being avascular, as expected (4). 2) The choroidal vasculature has markedly higher blood flow and blood volume than the retinal vasculature, consistent with established differences in blood flow between the two vasculatures (2,5). 3) The Gd-DTPA enhanced strip associated with the choroidal vascular layer and the vascularized tapetum is apparently thicker than the Gd-DTPA enhanced strip associated with the retinal vascular layer closest to the vitreous. These results suggest that the projection of capillary bed from the retinal vasculature into the bipolar cell layer may be sparse. In short, the Gd-DTPA experiments further corroborated the T_2 and diffusion imaging findings and set the upper limits on retinal thickness.

The MRI-estimated total thickness of the retina, including the tapetum and choroid vascular layer, was 358 ± 13 μm. These total thicknesses were slightly thicker than the total retinal thickness by histology (319 ± 77 μm). Cognizant of the partial-volume effect, we estimated the MRI-derived neural retinal thickness to be ~239 μm, in reasonable agreement with published histological data (neural retina: 150–250 μm) (13,32,34,35) but slightly larger than our histology (neural retina: 184 ± 33 μm). There are many factors that could account for the difference between MRI and histology data. They include, but not limited to, different slice being compared, laminar thickness in the retina being highly variable, shrinkage associated with fixation, and limited MRI spatial resolution. Shrinkage associated with the fixative processes is likely to yield a lower limit on thickness, underscoring the importance of in vivo measurements.

We did not find any published literature on the thickness of cat tapetum and the literature on the thickness of the choroidal vascular layer in cats is sparse. This is not surprising because the thin choroidal vascular layer detach easily which could lead to overestimation of thickness. We reported a tapetum thickness of 87 ± 35 μm and choroidal vascular layer thickness of $82 \pm$

14 μm by histology. Choroidal vascular layer thickness had been reported to range from 75 to 100 μm (36). The retinal vascular layer is embedded within the ganglion cell layer with projected capillary bed into the bipolar cell layer (1), and it does not constitute a separate layer. In short, the retinal thickness, cell layer assignments, and retinal and choroid vasculature assignments are in reasonable agreement with histology herein and the published histological data.

In conclusion, laminar structures and vascular layer of the retina were resolved using multiple MRI contrasts. To the best of our knowledge, this is the first MRI study demonstrating unequivocal laminar structures in the retina. Further improvements are expected. MRI has the potential to provide lamina-specific anatomical, physiological (such as tissue blood flow and oxygenation) and functional information on the retina in a single setting without depth limitation and, thus, it could complement existing techniques to study the retina and the entire visual pathway.

ACKNOWLEDGEMENTS

REFERENCES

1. Wassle H, Boycott BB. Functional architecture of the mammalian retina. Physiol Rev 1991;1:447–480.
2. Sharma RJ, Ehinger BEJ. Development and structure of the retina. In: Kaufman PL, Alm A, editors. Alder's physiology of the eye. St. Louis, MO: Mosby; 1992. p 319–348.
3. Ollivier FJ, Samuelson DA, Brooks DE, Lewis PA, Kallberg ME, Komaromy AM. Comparative morphology of the tapetum lucidum (among selected species). Vet Ophthalmol 2004;7:11–22.
4. Harris A, Kagemann L, Cioffi GA. Assessment of human ocular hemodynamics. Surv Ophthalmol 1998;42:509–533.
5. Bill A. Circulation in the eye. In: Renkin EM, Michel CC, editors. Handbook of physiology: cardiovascular. Bethesda, MD: American Physiological Society; 1984.
6. Montenegro MH. Retinal blood flow in diabetes. Int Ophthalmol Clin 1998;38:103–110.
7. Alder VA, Su EN, Yu DY, Cringle S, Yu P. Overview of studies on metabolic and vascular regulatory changes in early diabetic retinopathy. Aust N Z J Ophthalmol 1998;26:141–148.
8. Harris A, Chung HS, Ciulla TA, Kagemann L. Progress in measurement of ocular blood flow and relevance to our understanding of glaucoma and age-related macular degeneration. Prog Retin Eye Res 1999;18:669–687.
9. Lutty G, Grunwald J, Majji AB, Uyama M, Yoneya S. Changes in choriocapillaris and retinal pigment epithelium in age-related macular degeneration. Mol Vis 1999;5:35.
10. Ciulla TA, Danis RP, Harris A. Age-related macular degeneration: a review of experimental treatments. Surv Ophthalmol 1998;43:134–146.
11. Brown KT, Wiesel TN. Localization of the origins of the electroretinogram components by intraretinal recording in the intact cat eye. J Physiol 1961;158:257.
12. Sutter EE, Tran, D. The field topography of ERG components in man. I. Vis Res 1992;32:433–446.
13. Linsenmeier RA. Effects of light and darkness on oxygen distribution and consumption in the cat retina. J Gen Physiol 1986;88:521–542.
14. Yu D-I, Cringle SJ, Alder V, Su E-N. Intraretinal oxygen distribution in the rat with graded systemic hyperoxia and hypercapnia. Invest Ophthalmol Vis Sci 1999;40:2082–2087.
15. Shonat RD, Wilson DF, Riva CE, Pawlowski M. Oxygen distribution in the retinal and choroidal vessels of the cat as measured by a new phosphorescence imaging method. Appl Optics 1992;31:3711–3718.
16. Grinvald A, Bonhoeffer T, Vanzetta I, Pollack A, Aloni E, Ofri R, Nelson D. High-resolution functional optical imaging: from the neocortex to the eye. Ophthalmol Clin North Am 2004;17:53–67.
17. Zarella MD, Li H, Kwon Y, Kardon R, Soliz P, Tso DY. The origins and spatio-temporal properties of stimulus dependent intrinsic optical signals of the retina. In: Society for Neuroscience, 2004. Program No. 934.910.
18. Tsunoda K, Oguchi Y, Hanazona G, Tanifuji M. Mapping cone- and rod- induced retinal responsiveness in macaque retina by optical imaging. Invest Ophthalmol Vis Sc 2004;45:3820–3826.
19. Preussner PR, Richard G, Darrelmann O, Weber J, Kreissig I. Quantitative measurement of retinal blood flow in human beings by application of digital image-processing methods to television fluorescein angiograms. Graefes Arch Clin Exp Ophthalmol 1983;221:110–112.
20. Blair NP, Feke GT, Morales-Stoppello J, Riva CE, Goger DG, Collas G, McMeel JW. Prolongation of the retinal mean circulation time in diabetes. Arch Ophthalmol 1982;100:764–768.
21. Guyer DR, Yannuzzi LA, Slakter JS, Sorenson JA, Orlock S. The status of indocyanine-green videoangiography. Curr Opin Ophthalmol 1993;4:3–6.
22. Schmidt-Erfurth U. Indocyanine green angiography and retinal sensitivity after photodynamic therapy of subfoveal choroidal neovascularization. Semin Ophthalmol 1999;144:35–44.
23. Webb RH, Hughes GW. Scanning laser ophthalmoscope. IEEE Trans Biomed Eng 1981;28:488–492.
24. Hee MR, Izatt JA, Swanson EA, et al. Optical coherence tomography of the human retina. Arch Ophthalmol 1995;113:325–332.
25. Fujimoto JG, Pitris C, Boppart SA, Brezinski ME. Optical coherence tomography: an emerging technology for biomedical imaging and optical biopsy. Neoplasia 2000;2:9–25.
26. Berkowitz BA, Wilson CA, Hatchell DL, London RE. Quantitative determination of the partial oxygen pressure in the vitrectomized rabbit eye in vivo using 19F NMR. Magn Reson Med 1991;21:233–241.
27. Berkowitz BA, Wilson CA. Quantitative mapping of ocular oxygenation using magnetic resonance imaging. Magn Reson Med 1995;33:579–581.
28. Ogawa S, Lee T-M, Nayak AS, Glynn P. Oxygenation-sensitive contrast in magnetic resonance image of rodent brain at high magnetic fields. Magn Reson Med 1990;14:68–78.
29. Duong TQ, Ngan S-C, Ugurbil K, Kim S-G. Functional Magnetic Resonance Imaging of the Retina. Invest Ophthalmol Vis Sci 2002;43:1176–1181.
30. Duong TQ. Physiological modulation of fMRI signal in the retina high-resolution. In: Proceedings of the 10th Annual Meeting of ISMRM, Honolulu, HI, USA, 2002. p 1369.
31. Duong TQ, Kim D-S, Ugurbil K, Kim S-G. Spatio-temporal dynamics of the BOLD fMRI signals in cat visual cortex: Toward mapping columnar structures using the early negative response. Magn Reson Med 2000;44:231–242.
32. Buttery RG, Hinrichsen CFL, Weller WL, Haight JR. How thick should a retina be? A comparative study of mammalian species with and without intraretinal vasculature. Vision Res 1991;31:169–187.
33. LeBihan D, Breton E, Lallemand D, Aubin ML, Vitnaud J, Laval-Jeantet M. Separation of diffusion and perfusion in intravoxel incoherent motion MR imaging. Radiology 1988;168:497–505.
34. Prince JH, Diesem CD, Eglitis I, Ruskell GL. Anatomy and histology of the eye and orbit in domestic animals. Springfield, IL: Charles C Thomas; 1960. p 370.
35. Landers MB, 3rd. Retinal oxygenation via the choroidal circulation. Trans Am Ophthalmol Soc 1978;76:528–556.
36. Tansley K, editor. Vision in vertebrates. London: Chapman & Hall; 1965. 272 p.
37. Shen Q, Ren H, Bouley J, Fisher M, Duong TQ. Dynamic tracking of acute ischemic tissue fates using improved unsupervised ISO-DATA analysis of high-resolution quantitative perfusion and diffusion data. J Cereb Blood Flow Metab 2004;24:887–897.